Impact of Magnets on Ferrofluid Cooling Process: Experimental and Numerical Approaches

Sleimane Nasser El Dine [1], Xavier Mininger[1], Caroline Nore[2], Raphaël Zanella[1,2,3], Frédéric Bouillault [1], and Jean-Luc Guermond[3]

[1]GeePs, CNRS, CentraleSupélec, Univ. Paris Sud, Université Paris-Saclay, Sorbonne Université, 91192 Gif-sur-Yvette, France
[2]LIMSI, CNRS, Univ. Paris Sud, Université Paris-Saclay, 91405 Orsay, France
[3]Department of Mathematics, Texas A&M University, College Station, TX 77843 USA

The cooling performance of vegetable oil seeded with ferromagnetic nanoparticles is tested on a prototype electric transformer coil. The system is investigated both experimentally and numerically. The numerical simulations are done with finite elements assuming axisymmetry. The experimental and numerical results match very well with each other. The numerical tool is also used to investigate the impact of an annular magnet enclosing the setup. The orientation of the remanent magnetic induction of the magnet is observed to play a significant role in determining the cooling efficiency.

Index Terms— Cooling, ferrofluid, finite-element method, magnet, thermomagnetic convection.

I. Introduction

EXCESSIVE heating of power transformers is known to compromise the longevity of these devices. A possible solution to this problem consists of using ferrofluids as cooling agents to enhance the heat-transfer rate. A ferrofluid is a stable colloidal suspension of ferromagnetic nanoparticles dispersed in a non-magnetic carrier liquid. In this article, we study the heat-transfer properties of a ferrofluid composed of Midel vegetable oil seeded with cobalt ferrite $CoFe_2O_4$ nanoparticles. At constant magnetic field, the magnetic permeability of a hot ferrofluid is smaller than that of a cold one [1]. The relation between the ferrofluid magnetization and magnetic field is taken into account by using the assumption of a linear magnetic material for ferrofluids [2]

$$\mathbf{M} = \chi(T)\mathbf{H} \tag{1}$$

where $\mathbf{M}$ is the ferrofluid magnetization, T the temperature, and $\mathbf{H}$ is the magnetic field. Here, χ is the magnetic susceptibility of the ferrofluid and, as shown in the following, it depends on a number of parameters:

$$\chi(T) = \frac{\phi \mu_0 \pi d^3 M_{s,p}^2(T)}{18 k_B T}, \quad \frac{M_{s,p}(T)}{M_0} = 1 - \left(\frac{T}{T_c}\right)^{\frac{3}{2}} \tag{2}$$

where ϕ is the volume fraction of magnetic material, μ_0 the vacuum magnetic permeability, d the particle average diameter, $M_{s,p}(T)$ the temperature-dependent particle magnetization, k_B the Boltzmann's constant, M_0 the particle magnetization at saturation and at 0 K, and T_c the Curie temperature of the cobalt ferrite nanoparticles. The magnetic force added to the thermal buoyancy force changes the flow pattern in

the tank. The heated ferrofluid loses its magnetization near the transformer windings and is pushed up by the magnetic and relatively cooler fluid from the surroundings. After losing its heat, the magnetic fluid regains its magnetization. This process helps transfer the heat from the transformer windings to the external shell of the transformer, where the heat is eventually exchanged with ambient air [3]. This mechanism is called thermomagnetic convection. The magnetic force can be modeled by the Helmholtz force (in N/m³)

$$\mathbf{F} = -\mu_0 \frac{H^2}{2} \nabla \chi(T) \tag{3}$$

where $H = \|\mathbf{H}\|$. This force connects the variations in the magnetization with the thermal gradient. Therefore, if effective, one expects that the thermomagnetic convection can help avoid using external mechanical pumping systems.

This article is organized as follows. We first present in Section II the experiment investigated in this article and review the equations modeling the system. The setup is composed of a coil immersed in a ferrofluid. Then, we describe in Section III the finite-element code that is used to solve the coupled thermo-magnetohydrodynamics system. The numerical results and experimental ones are compared in Section IV. After cross-validating the experimental and the numerical results, we numerically study the impact of an annular magnet on the cooling process.

II. Experimental Setup and Governing Equations

A. Experimental Setup

The experimental setup under study consists of a copper coil immersed in a ferrofluid contained in a cylindrical tank made of aluminum. The tank is closed at the top by a polyvinyl chloride (PVC) cap as shown in Fig. 1. An annular magnet enclosing the tank can be added at different heights in order to study its impact on the cooling process. The setup dimensions are given in Table I.
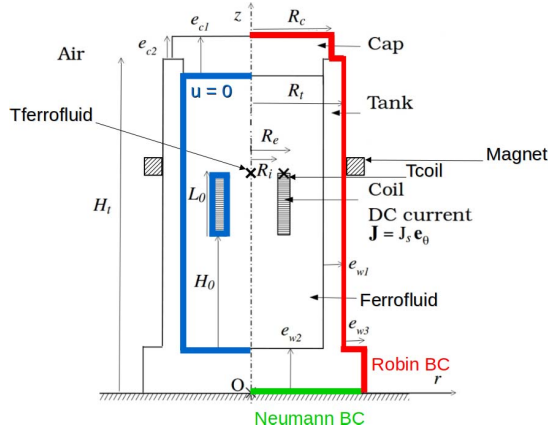
Fig. 1.   Experimental setup using ferrofluid cooling.

TABLE I
EXPERIMENTAL SETUP DIMENSIONS

Parameter	H_t	R_t	e_{w1}	e_{w2}	e_{w3}	H_0
Value (cm)	12.5	3.1	1	2	1	3.9
Parameter	L_0	R_i	R_e	R_c	e_{c1}	e_{c2}
Value (cm)	2.1	0.8	1.175	2.6	2	1

B. Governing Equations

The magnetic fluid is considered as a homogeneous continuous medium with incompressible Newtonian fluid behavior. The study of the thermal exchanges through the cooling device requires the knowledge of the velocity field, which we assume to be well modeled by the Navier–Stokes equations

$$\begin{cases} \nabla \cdot \mathbf{u} = 0 \\ \rho_l \frac{D\mathbf{u}}{Dt} + \nabla p - \nabla \cdot \mathbb{e}(T, \mathbf{u}) = \rho_l \beta g(T - T_{\text{ext}})\mathbf{e}_z + \mathbf{F} \end{cases} \quad (4)$$

where $\mathbf{u}$ is the velocity vector, $\mathbb{e}(T, \mathbf{u}) = \eta(T)(\nabla \mathbf{u} + (\nabla \mathbf{u})^{\mathrm{T}})$, D/Dt the material derivative, p the pressure, η is the dynamic viscosity (given by $\eta(T) = Af(\phi)\exp(BT^{-1})$ with $A = 1.3 \times 10^{-6}$ Pa $\cdot$ s, $B = 3.1 \times 10^3$ K and $f(\phi)$ given by Rosensweig's model, see [4, p. 105]), ρ_l the density, β the thermal expansion coefficient, g the gravity, T the temperature, and T_{ext} the reference temperature. The last two terms on the right-hand side of the momentum equation are, respectively, the buoyancy force and the magnetic force. The heat-transfer process that occurs in the ferrofluid is described by the heat equation

$$\rho_l C_p \frac{DT}{Dt} = \nabla \cdot (\lambda \nabla T) + Q \quad (5)$$

where C_p is the specific heat capacity at constant pressure, λ the thermal conductivity, and Q the volumic heat source dissipated by Joule effect at the coil and given by $(1/\sigma)J_s^2$ (where σ is the copper electrical conductivity, and J_s the current density in the coil).

The computed electromagnetic field is assumed to be steady, and the ferrofluid magnetization is considered as instantaneously aligned with the magnetic field [4, pp. 22–23].

The pyromagnetic coefficient is neglected. The magnetostatic equations are given by

$$\nabla \times \mathbf{H} = \mathbf{J}, \quad \nabla \cdot (\mu \mathbf{H}) = 0, \quad \mu = \mu_0(1 + \chi(T_{\text{ext}})) \quad (6)$$

where $\mathbf{J} = J_s\mathbf{e}_\theta$ and μ is the magnetic permeability of the ferrofluid. Recall that χ is given by (2) and μ_0 is the magnetic permeability of vacuum.

Numerically, the PVC-aluminum tank is enclosed in a larger cylinder of radius 0.1 m and height 0.2 m and is therefore surrounded by a specific volume of ambient air. At the boundaries of this cylinder, the boundary condition for the magnetic problem $\mathbf{H} \times \mathbf{n} = \mathbf{0}$ is enforced. The non-slip boundary condition $\mathbf{u} = \mathbf{0}$ is applied at the boundary of the fluid domain (see blue lines in Fig. 1). The air convection at the top and on the lateral wall of the PVC-aluminum tank is modeled by using a Robin boundary condition on the temperature

$$-\lambda \nabla T \cdot \mathbf{n} = h(T - T_{\text{ext}}) \quad (7)$$

where h is the convection coefficient and $\mathbf{n}$ is the outer unit normal vector (see red lines in Fig. 1). The homogeneous Neumann boundary condition $\partial_z T = 0$ is enforced at the bottom of the tank (see green line in Fig. 1). The initial conditions are $\mathbf{u} = \mathbf{0}$, $T = T_{\text{ext}}$, and $\mathbf{H} = \mathbf{0}$.

III. SFEMaNS CODE

We use the code SFEMaNS (the acronym stands for spectral/finite elements for the Maxwell and Navier–Stokes equations) for solving the coupled system of the aforementioned equations. We use a Fourier decomposition in the azimuthal θ-direction and continuous finite elements in the meridian section (piecewise linear Lagrange elements for the pressure and piecewise quadratic Lagrange elements for the velocity, the magnetic field, and the temperature). For instance, the approximate temperature field has the following representation:

$$T = \sum_{m=0}^{m_{\max}-1} T_m^c(r, z, t)\cos(m\theta) + \sum_{m=1}^{m_{\max}-1} T_m^s(r, z, t)\sin(m\theta) \quad (8)$$

where $T_m^c(r, z, t)$ and $T_m^s(r, z, t)$ are scalar-valued finite-elements functions and $m_{\max}$ is the number of (complex) Fourier mode used in the discretization. All of the fields, either vector-valued or scalar-valued, are represented as shown in (8). Modulo the computation of non-linear terms using FFTW, the handling of the Fourier modes in the meridian plane, (r, z), can be done in parallel. The divergence of $\mu \mathbf{H}$ is controlled by a technique using a negative Sobolev norm that guarantees convergence under minimal regularity. SFEMaNS has been thoroughly validated on numerous analytical solutions and against other magnetohydrodynamics codes [5], [6]. All of the computations reported in this article are done assuming axisymmetry, i.e., $m_{\max} = 1$.

IV. RESULTS AND COMPARISONS

A. Experiment Versus Numerics for the Coil Experiment

The copper coil that we use is doubly winded in order to form two coaxial resistors. When the direction of the
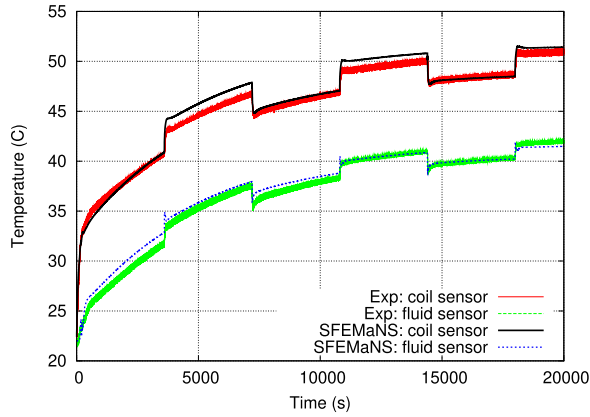
Fig. 2. Experimental and numerical temperature measurements with alternating magnetic force: the Helmholtz force is operative for $0 \leq t < 3600$ s and switched off for 3600 s $\leq t < 7200$ s with a total period of 7200 s.

TABLE II

PROPERTIES USED IN THE SIMULATIONS

Property	Cu	Al	PVC	Coil	Ferrofluid
Density (kg/m^3)	8933	2.70e3	1.40e3	4.00e3	1.115e3
Therm. expansion (/K)	-	-	-	-	6.62e-4
Heat capacity (J/K·kg)	385	945	1e3	612.82	1.685e3
Therm. cond. (W/m·K)	401	201	0.16	0.404	0.186
Dyn. viscosity (Pa.s)	-	-	-	-	0.0787

current I is the same in the two windings (the magnetic field produced by the coil is non-zero), both the Joule effect and the Helmholtz force are operative. When the direction of the current is opposite in the windings, only the Joule effect is operative. We can therefore highlight the action of the Helmholtz force in the same experimental configuration.

Temperatures are continuously measured at two locations: on the coil and in the fluid on the symmetry axis (see the symbols "Tcoil" and "Tferrofluid" in Fig. 1). The Helmholtz force is periodically switched on and off with a total period of 7200 s, starting with an active force at $t = 0$ s. The time evolution on the two sensors is shown in Fig. 2.

The physical properties used for the Navier–Stokes and heat equations are listed in Table II. The ambient air is characterized by the exterior temperature $T_{ext} = 295.15$ K and the heat-transfer coefficient $h = 6.5$ W/m^{2}K. The other parameters are $\phi = 5.4\%$, $d = 16$ nm, $M_0 = 3.87 \times 10^5$ Am^{-1}, and $T_c = 793$ K. The electrical current in the coil is $I = 8$ A with the density $J_s = 3.35 \times 10^6$ Am^{-2}, electrical conductivity $\sigma = 5.998 \times 10^7$ Sm^{-1}, and the number of windings $N = 33$. The meridian mesh contains $118\,451$ nodes. The time step 0.025 s is used over 9×10^5 iterations (about 25 wall-clock hours using 64 processors for the domain decomposition on the cluster IBM x3750-M4 from GENCI-IDRIS).

Some uncertainties on the values of the physical parameters exist. However, the agreement between the experimental measurements of the temperatures on the two sensors and the numerical computations is excellent and therefore validates our ferrofluid modeling. Snapshots of the numerical velocity and temperature fields at $t = 16\,000$ s (when the Helmholtz force is active) and $t = 20\,000$ s (when the Helmholtz force
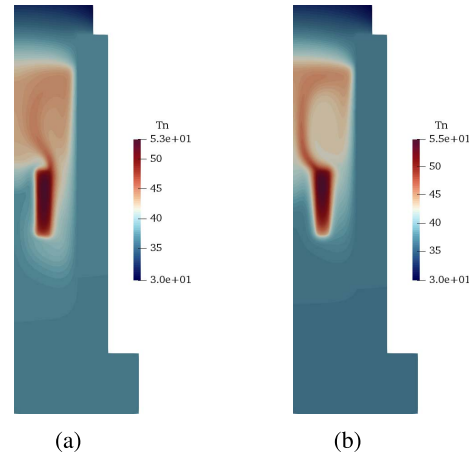

Fig. 3. Temperature field (in Celsius) with alternating magnetic force. The symmetry axis (Oz) is on the left. (a) Helmholtz force at $t = 16\,000$ s. (b) No Helmholtz force at $t = 20\,000$ s.
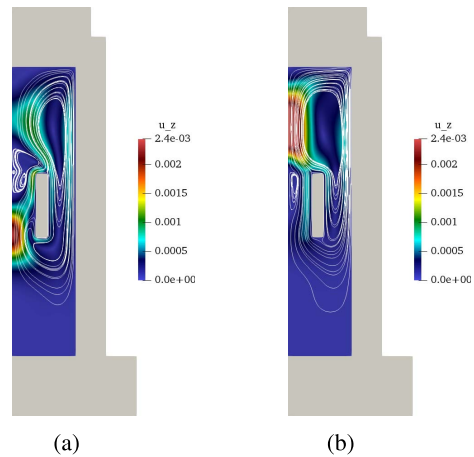

Fig. 4. Color maps of the vertical velocity (in ms^{-1}) and velocity streamlines with alternating magnetic force. The symmetry axis (Oz) is on the left. The PVC-aluminum tank is shown in gray. (a) Helmholtz force at $t = 16\,000$ s. (b) No Helmholtz force at $t = 20\,000$ s.

is inactive) are shown in Figs. 3 and 4. Fig. 3 shows that the Helmholtz force has an impact of the thermal plume. When the Helmholtz force is active, the plume is deviated in the bulk above the coil, whereas it is centered on the symmetry axis when the Helmholtz force is switched off. This deviation is due to a recirculation localized near the bottom of the coil which pushes the hot fluid away from the axis [see Fig. 4(a)]. This lower recirculation does not exist when the Helmholtz force is inactive: the buoyancy force alone generates a single recirculation in the top part of the tank [see Fig. 4(b)]. Notice that the maximum value of the vertical velocity is the same with or without the Helmholtz force, but the maximum value of the temperature is lowered by 2 K when the Helmholtz force is operative. This proves that the thermomagnetic convection mechanism is beneficial in this case.

B. Numerical Results for the Ferrofluid Experiment With Coil and Magnet

We now numerically study the impact of an annular magnet with a remanent induction amplitude of 0.3 T. The magnet is localized alongside the PVC-aluminum tank. The objective is
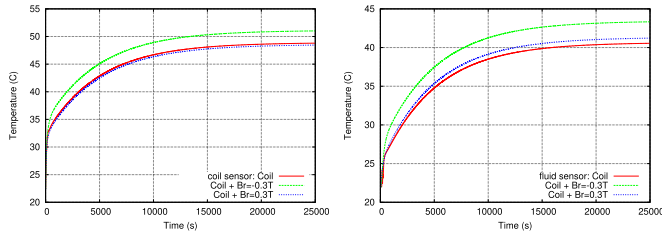
Fig. 5. Comparison of the temperatures computed at the two sensors for the three cases: only coil (red line), coil and $B_r = -0.3$ T (green line), and coil and $B_r = +0.3$ T (blue line).
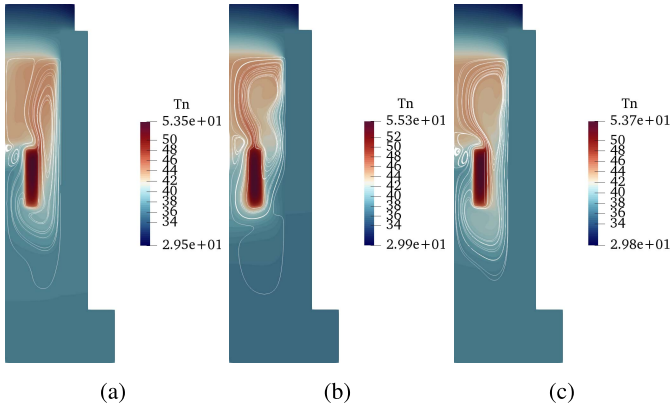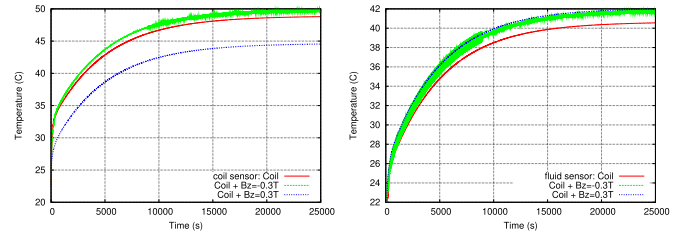

Fig. 7. Comparison of the temperatures computed at the two sensors for the three cases: only coil (red line), coil and $B_z = -0.3$ T (green line), and coil and $B_z = +0.3$ T (blue line).

Fig. 6. Temperature field (in Celsius) and velocity streamlines at $t = 25\,000$ s for the three cases. (a) Only coil. (b) $B_r = -0.3$ T and coil. (c) $B_r = +0.3$ T and coil.
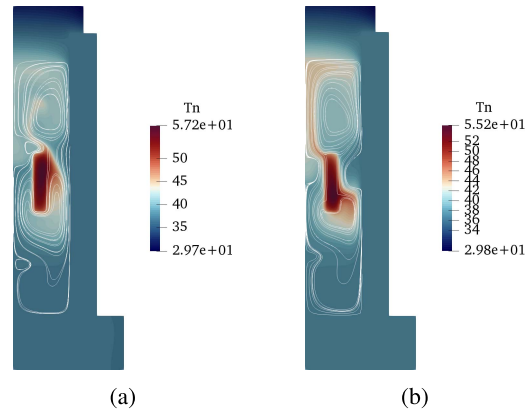

Fig. 8. Temperature field (in Celsius) and velocity streamlines at $t = 25\,000$ s with the coil and annular magnet $B_z = \pm0.3$ T. (a) $B_z = -0.3$ T and coil. (b) $B_z = +0.3$ T and coil.

to use the magnet to improve the cooling by changing the distribution of the magnetic field induced by the coil.

1) Magnet With a Radial Remanent Induction Field: We test the action of an annular magnet of rectangular cross section with $B_r = \pm0.3$ T, inner radius $r_i = 3.1$ cm, outer radius $r_o = 3.6$ cm, and height 1 cm. The bottom inner corner is localized at $r = 3.1$ cm and $z = 8$ cm (see Fig. 1). Fig. 5 shows the time evolution of the temperature at the two sensors. Using $B_r = +0.3$ T produces very little changes, whereas using $B_r = -0.3$ T increases the temperature at both sensors by approximately 3 K. Fig. 6 shows the temperature field in the saturated regime for the three cases. Hence, adding an annular magnet with a radial remanent induction does not decrease the maximum temperature reached in the coil.

2) Magnet With a Vertical Remanent Induction Field: We now test the action of an annular magnet with $B_z = \pm0.3$ T using the same geometry and location of the magnet as in Section IV-B1. Fig. 7 shows the time evolution of the temperature at the two sensors. Using $B_z = -0.3$ T leads to an oscillating state (with a period of 22 s for $t < 9000$ s and 44 s for $t \geq 9000$ s). Using $B_z = +0.3$ T yields a steady state with a strong decrease of the temperature at the coil sensor. In fact, the maximum temperature observed in Fig. 8(b) is larger than the maximum temperature obtained with the coil alone by 1.7 K [see Fig. 6(a)].

To conclude, the temperature and velocity fields are strongly impacted by an annular magnet with a ±0.3 T remanent induction field. Optimization of the location, strength, and orientation of the magnet will be done in the near future. We are also going to extend our investigations to more realistic configurations of power transformers like in [4, pp. 127–154].

REFERENCES

[1] M. Petit, A. Kedous-Lebouc, Y. Avenas, W. Cherief, and E. Rullière, "Etude expérimentale d'un système statique de génération de pression magnétothermique," in *Proc. Symp. de Génie Électrique*, Jul. 2014, pp. 1–6.

[2] R. Zanella, C. Nore, F. Bouillault, J.-L. Guermond, and X. Mininger, "Influence of thermomagnetic convection and ferrofluid thermophysical properties on heat transfers in a cylindrical container heated by a solenoid," *J. Magn. Magn. Mater.*, vol. 469, pp. 52–63, Jan. 2019.

[3] J. Patel, K. Parekh, and R. V. Upadhyay, "Prevention of hot spot temperature in a distribution transformer using magnetic fluid as a coolant," *Int. J. Therm. Sci.*, vol. 103, pp. 35–40, May 2016.

[4] R. Zanella, "Thermomagnetic convection in ferrofluids: Finite element approximation and application to transformer cooling," Ph.D. dissertation, Univ. Paris Saclay, Saint-Aubin, France, 2018.

[5] C. Nore, H. Zaidi, F. Bouillault, A. Bossavit, and J.-L. Guermond, "Approximation of the time-dependent induction equation with advection using Whitney elements," *COMPEL-Int. J. Comput. Math. Elect. Electron. Eng.*, Vol. 35, no. 1, pp. 326–338, 2016.

[6] A. Giesecke *et al.*, "Influence of high-permeability discs in an axisymmetric model of the Cadarache dynamo experiment," *New J. Phys.*, vol. 14, no. 5, May 2012, Art. no. 053005.